CE 5963 – Undergraduate Research Thesis

Information and Tentative Outline

Fall 2015 to Winter 2016

Specific to Students under Supervision of

Dr. Alan Lloyd

CE 5963– Undergraduate Research Thesis
Fall 2015 – Winter 2016

Supervisor	Dr. Alan Lloyd
Email	Alan.Lloyd@unb.ca
Office	Head Hall HC4

Course Description from Calendar

The research thesis is an independent project conducted under the supervision of a faculty member over a period of two sequential semesters. Students are responsible for finding a supervisor and initiating the project. Suitable projects may include experimental investigations, field investigations, design projects, computational projects, software development or feasibility studies. Deliverables include a detailed proposal, periodic progress reports, a comprehensive dissertation and an oral presentation.

Prerequisites from Calendar

1. CE 3973 (Co-requisite)
2. Restricted to students with 100 ch completed and with a GPA of 3.3 in the previous assessment year or a CGPA of 3.3.

Other Requirements and Limitations

1. Students are only accepted at discretion of Dr. Alan Lloyd
2. Certain topics may have prerequisites in addition to the ones outlined in the calendar. For example, a research project in reinforced concrete will require students to have taken CE 3053.
3. An experimental research project may require students to commit to working around the hours of the technician.
4. All projects require students who are motivated and capable of self-directed study.

Deliverables	**Term 1**	**Term 2**
Weekly Deliverables	30-60 minute meeting	30-60 minute meeting
	Progress update and work report	Progress update and work report
Major Deliverables	Letter of Intent	Dissertation
	Proposal	Presentation

Item	Brief Description
Weekly Meetings	These will be 30-60 minutes in duration at a minimum with additional time if needed. As the project begins, this time will be largely information flowing from the supervisor to the student. As the project progresses, this is expected to switch with the student taking the time to update the supervisor on the project.
Progress Update and Work Report	The student will keep a record of time spent on major tasks. This will be compiled in tabular and graphical format and be regularly updated throughout the terms. This document will ensure that both the student and the supervisor understand the time and work commitment of the project.
Letter of Intent	Once a student and the supervisor have agreed to a project, the student is required to submit a letter of intent. This letter should demonstrate that the student: 1) Understands his or her requirements for the project 2) Understands the scope of the project 3) Can clearly state the objectives and research expectations of the project The letter should also contain the following items: 1) An up to date curriculum vitae (CV) 2) A brief description of career goals
Proposal and Presentation	This document is the major deliverable from the first term. It is expected to become part of the thesis and should contain: 1) Literature review on the research topic 2) Proposed research scope 3) Proposed research methodology 4) Expected outcomes of the research A student is expected to have made some progress on the actual research (beyond what is listed above) by the end of the first semester. This progress may or may not be included in the proposal as well. At the end of the student will make a presentation of the proposed research to some members of the faculty and graduate students working in complementary areas. This will allow the student to receive constructive feedback that may be useful in the research project.
Dissertation	This document is the major deliverable of the second term (and the project as a whole). It is to be a comprehensive description of the research conducted. There is a very high expectation for quality of presentation of work including writing structure, format, figure quality, and table quality. The thesis will generally contain the following chapters: 1) Introduction • Summarize the project and state objectives 2) Background and theory • Literature review of past research

	• Discussion of theoretical concepts used in experiment and analysis 3) Research Program • Detailed description of the research that will be preformed • If experimental, it will describe the specimens, test setup, and instrumentation • If analytical, it will describe analyses method, software, etc. 4) Experimental Results • Presentation of the results of the tests • Quantitative (numbers, graphs, tables) • Qualitative (pictures, figures, descriptions) 5) Assessment of Results • Comparison of results • Discussions • Sources of error 6) Conclusions • Major and minor findings of the research 7) Formatted Conference Paper* • See the conference paper section
Presentation	An oral presentation (10-15 minutes) made to your peers that covers all aspects of your project

Conference Paper

The major goal of research is to further the state of the art of the topic. This is not possible without making an effort to disseminate results. Therefore, projects are intended to produce publishable results. In cases where publication is possible, it will be in the form of a conference paper. Writing this paper will be a requirement of all projects and the paper will be included in the dissertation document. The CSCE annual conference will be used as a template for the paper requirements for this project.

Conference Papers:

- Are approximately 10 pages long
- Are well written and concise
- Contain information that is new and worthy of publication

Notes if the paper is published

- The student will be the primary author. This will be valuable to students who are looking for employment or applying to graduate studies.
- Although the paper may be published in a conference, there should be *no expectation that the student will attend the conference.* There is no funding in place for this.

The following pages contain:

1) An example of a conference paper that is primarily based on experimental research.
2) An example of a conference paper that is based on analytical research.

2nd International Engineering Mechanics and Materials Specialty Conference
le 2e Congrès international de mécanique et des matériaux

Ottawa, Ontario
June 14-17, 2011 / 14 au 17 juin 2011

High Strain-Rate Effects on the Dynamic Material Properties of Wood Beams

Alan Lloyd[1], Eric Jacques[1], Omar Abdelalim[2], Murat Saatcioglu[3], Abass Braimah[2], and Ghasan Doudak[1]

1. Department of Civil Engineering, University of Ottawa, Ottawa, Ontario, Canada
2. Department of Civil and Environmental Engineering, Carleton University, Ottawa, Ontario, Canada

Abstract: Design and construction of structures for blast safety requires an understanding of material properties under high rates of strain. A dynamic increase factor (DIF) – defined as the ratio of dynamic to static material property – is used to quantify the observed strain-rate dependence of material characteristics. The DIF is relatively well defined for common blast resistant construction materials, such as reinforced concrete and steel. However, little attention has been directed towards understanding the behaviour of wood members under rapid loading rates. A joint experimental research program between the University of Ottawa and Carleton University is currently underway to investigate the strain-rate dependence of the modulus of elasticity and modulus of rupture of sawn lumber specimens. A total of thirty-six *Stud grade 2"×6"* spruce-pine-fir (S-P-F) members were tested under four point bending at static and high strain-rates (on the order of *0.3 s*$^{-1}$). The University of Ottawa's shock tube was used to generate shock wave loading while the static testing was carried out in the structures laboratory of Carleton University. Strains, displacements and applied loads were measured during static and high strain-rate testing. High speed video recordings of the response of the studs were also made and used to categorize failure modes. A single-degree-of-freedom numerical model was developed and used to characterize the material properties of S-P-F lumber under high rates of strain.

1. Introduction

Blast-resistant structures are usually designed to have the required strength under blast loads while ensuring ductility and continuity during response. Higher structural mass is also regarded as an asset in resisting blast loads. These properties can easily be achieved with reinforced concrete and structural steel framing systems. Even though wood construction is not generally thought to be blast-resistant, it is used extensively in Canada and may be subjected to blast loading from maliciously intended terrorist attacks or accidental explosions. Wood structures may also be subjected to blast loading due to their proximity to targeted high-profile buildings. Currently there is lack of knowledge on the dynamic material properties of wood under high strain-rates associated with blast loading. Furthering this knowledge is crucial to ensuring the proper design of wood structures that have a risk of explosive loading.

Most building material, especially concrete and steel, have been reported to exhibit increased strength under high strain-rates (Bischoff and Perry 1991, Malvar and Crawford 1998). Bischoff and Perry (1991) reported an increase in both the uniaxial compressive strength and stiffness of concrete under high strain-rate while Malvar and Ross (1998) reported similar behaviour when subjected to high uniaxial tension strain-rate. Malvar and Crawford (1998) carried out an experimental program to investigate the behaviour

of reinforcing steel under high strain-rate. The authors reported that unlike the compressive strength of concrete, only the tensile strength was affected by high strain-rate.

Currently, there is little information in the literature about the effect high strain-rates on the stress-strain characteristics of wood, especially at strain-rate levels experienced during blast loading. This paper describes an experimental research program designed to investigate the behaviour of wood specimen under high strain-rate. A summary of results of wood tested under static and nearly static strain-rates is presented. These static results are compared with the results of wood specimens tested under shock tube induced shock wave loading. The increase in both the apparent modulus of elasticity (MOE) and the modulus of rupture (MOR) of wood at high strain-rates is discussed.

2. Experimental Method

A total of *36 Stud grade 38 mm × 140 mm × 2440 mm* (*2"×6"×8'*) S-P-F wood specimens were tested. *18 specimens* were tested under static conditions at Carleton University and the remaining *18* were subjected to shock wave loading at the University of Ottawa. The specimens had average moisture contents by weight of *15.6 %* at the time of testing.

2.1. Typical Instrumentation

All specimens were tested under simply supported four-point bending to generate a constant moment region between the load application points. The distance between supports and the points of load application were *742.5 mm*, while the distance between load-application points was *750 mm*. Overall member length was *2440 mm*, with a clear span of *2235 mm*, or *16* times the dry depth of the member. *150 mm* long load bearing blocks were used at the location of the applied point loads. These bearing blocks had a radius of 560 mm (four times the depth of the specimens) and were used to ensure full contact between load bearing blocks and test specimens during testing. The configuration of a typical wood specimen is illustrated in Figure 1.

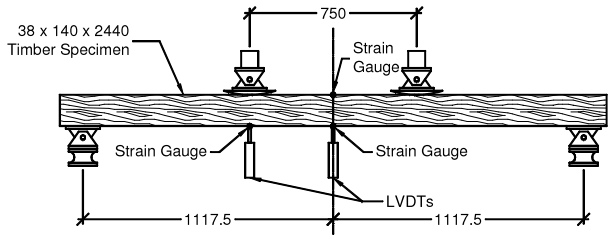

Figure 1: Typical Specimen Configuration and Instrumentation.

Specimens subjected to static and dynamic testing were instrumented in a similar manner. Three electrical resistance strain gauges were placed at the mid-point on the compression and tension sides and at one of the load points on the tension side to measure strain. Two linear variable displacement transducers (LVDTs) were used to measure deflection at the mid-point and at one of the load points. Under static testing, applied load was measured with a load-cell built integrally into the actuator. Under shock wave testing, two dynamic piezoelectric pressure sensors were used to measure the reflected pressure of the shock wave.

A high-speed digital oscilloscope was used as the data acquisition controller and was configured to record at *100,000 samples per second*. The data acquisition system was triggered and began recording data when the shock front passed over one of the pressure sensors. The data acquisition system recorded for a total duration of *3 seconds*. In addition to the specimen instrumentation, a high speed

camera was used to monitor the tests. This camera, set to record *500 frames per second*, was triggered by the data acquisition system such that video was synchronized with the recorded data-time history.

2.2. Static Test Set-up

During static testing a displacement-controlled actuator was used to apply two point loads to the specimens through a spreader beam. The wood specimen was braced at the ends and at the load points to prevent out-of-plane movement and warping. Figure 2 shows the static wood test setup and a wood specimen (a) before and (b) after testing.

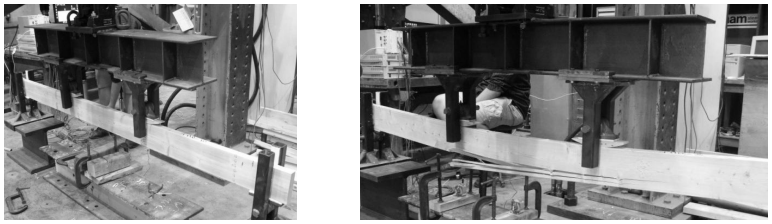

(a) Static specimen prior to testing. (b) Static specimen after testing.

Figure 2: Static testing of wood specimens.

2.3. Dynamic Test Set-up

Dynamic testing was performed at the University of Ottawa's Shock Tube Testing Facility. The University of Ottawa shock tube is capable of simulating explosive driven shock waves on structural components through the rapid release of compressed air. The pneumatically driven shock tube is composed of three main components: a variable length driver section, a spool section and an expansion section. The variable length driver and spool sections are shown in Figure 3 (a) while the expansion section and test frame are shown in Figure 3 (b). Shock wave energy is generated in the variable driver section, while firing is controlled by the spool section. The shock wave parameters – specifically the reflected pressure and reflected impulse – are controlled by selecting appropriate driver pressure and driver length combinations. The shock tube has an approximate maximum reflected pressure of *100 kPa* and reflected impulse of *2200 kPa-ms* (Lloyd, 2010).

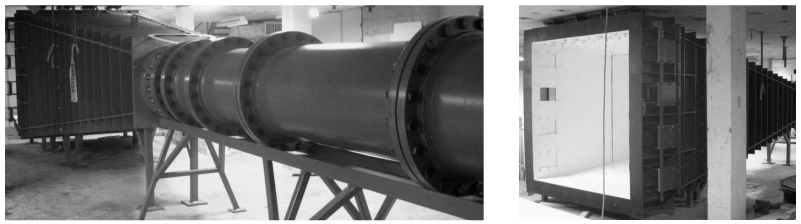

(a) Driver and spool sections (b) Expansion section with test frame

Figure 3: University of Ottawa Shock Tube.

A load transfer system was constructed to collect and apply shock wave pressures to the wood beams at two load points with similar spacing as in the static tests. The load transfer system consisted of two individual load transfer devices (LTD) which operated independently of each other. This system allowed for two specimens to be tested simultaneously. The load transfer devices were comprised of rigid steel

panels that collected and applied shock wave pressure to each specimen. Each load transfer device was *2032 mm* tall and *1000 mm* wide and, when placed side-by-side, completely covered the *2032 mm* by *2032 mm* opening at the front of the shock tube test frame. Sliding hinges increased the efficiency of the transfer system by permitting the entire load transfer device to freely translate laterally without causing a reaction at the hinge locations. A set of nylon ropes and steel wires were used to prevent excessive lateral deflections and rebound of the system into the shock tube. The entire system was capable of moving laterally a maximum of *200 mm*, had a mass of *101.8 kg* and each load transfer device had a tributary area of *1.7 m*^{2}. Details of the load transfer system are shown in Figure 4 (a) and (b), while a photograph of the system prior to testing is shown in Figure 4 (c).

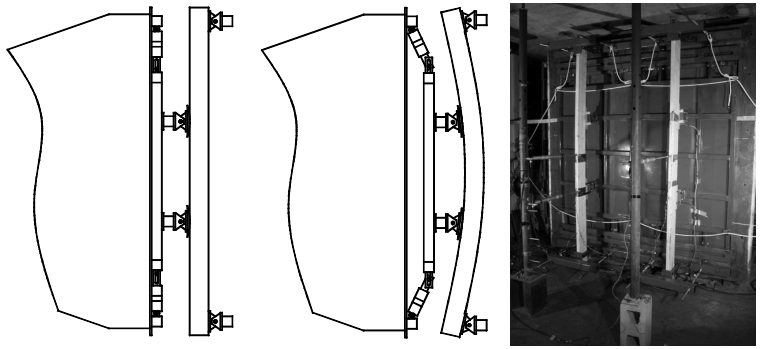

(a) LTD configuration prior to testing (b) LTD configuration during testing (c) Load transfer system

Figure 4: Details of the Load Transfer Device.

To facilitate direct comparison of test results obtained from dynamic testing, an effort was made to subject each specimen to the same reflected pressure-impulse combination. The preliminary shot on all specimens was performed with a driver length of *1220 mm* and driver pressure of approximately *207 kPa*. This generated a shock wave with reflected pressure of approximately *35 kPa*, positive phase duration of *10.8 ms* and reflected impulse of *175 kPa-ms*. The preliminary shot was selected on the basis of maximizing strain-rate and having the response of the specimen slightly exceed the modulus of rupture. As required, subsequent shots of higher reflected pressures and impulses were performed if the specimens did not fail. Typical specimen failure occurred between *5* and *25 ms* after the arrival of the shock front.

3. Preliminary Experimental Results

3.1. Static Results

A typical force-displacement relationship obtained from static testing of stud grade wood is shown in Figure 5. The shape of this curve is typical of the results achieved in this testing program. The behaviour shows a distinct elastic response up to the point of incipient failure. At which point, splitting or rupture of the section begins to occur at points of non-homogeneity, such as knots and other defects. Depending on the severity of the initial failure, the specimen may be able to resist some load as evidenced by the post-peak response in Figure 5. Often, several localized failures were observed prior to the global failure of the member. This behaviour is shown in Figure 5 where there were three instances of splitting or rupture that occurred prior to global member failure. Generally, the static specimens exhibited flexural (simple tension or cross-grained tension) failures.

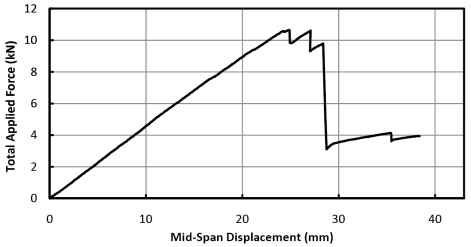

Figure 5: Typical Force-Displacement Relationship Obtained from Static Testing of Stud Grade Wood.

The static wood material properties of interest are the apparent modulus of rupture (MOR) and the apparent modulus of elasticity (MOE). These physical quantities are apparent as they are based on the global response of the beams, and not the properties at the location of failure. These two quantities will be compared with the same values derived from the dynamic testing. Using the recorded maximum applied force and corresponding displacement, the modulus of elasticity is solved for using Equation 1. The modulus of rupture (Eq. 3), which is the stress in the extreme fibre at maximum elastic load, is found by dividing the maximum moment (Eq. 2) by the elastic section modulus.

$$[1] \quad MOE = \frac{K_{avg} a (3L^2 - 4a^2)}{48I}$$

$$[2] \quad M_{\max} = \frac{P_{\max} a}{2}$$

$$[3] \quad MOR = SL \times \frac{M_{\max}}{S}$$

$$[4] \quad SL = 100.0 - 3.5 \log_{10} T_r$$

In Equation 1, K_{avg} is the apparent stiffness of the member, a is the distance between the support and the load point, L is the length of the member, and I is the moment of inertia of the section. In Equation 2, M_{max} and P_{max} are the moment and total load at failure. In Equation 3, SL is a correction factor to account for the static effect of load duration, defined in Equation 4 as a function of load duration (T_r in minutes), and S is the elastic section modulus (Karacabeyli and Barrett, 1993).

A summary of the corrected modulus of rupture and modulus of elasticity for *17* wood specimen tested under static conditions is shown in Figure 6 (a) and (b). All of the values for MOE and MOR have been adjusted for a loading rate of one minute to failure using Equation 4. In these figures, the apparent MOR and MOE given by the Canadian Wood Council (CWC) Lumber Properties Project (Barret and Lau, 1994) is also shown for comparison. The average MOR was found to be *37.4 MPa* with a standard deviation of *10.9 MPa* and a coefficient of variation of *29.1 %*. The average MOE was *9.2 GPa* with a standard deviation of *1.4 GPa* and a coefficient of variation of *14.9 %*. Both the average MOR and MOE were slightly larger than the CWC specified values of *35.2 MPa* and *9.0 GPa*, respectively, for Stud grade *38 mm × 140 mm* (*2"×6"*) S-P-F wood.

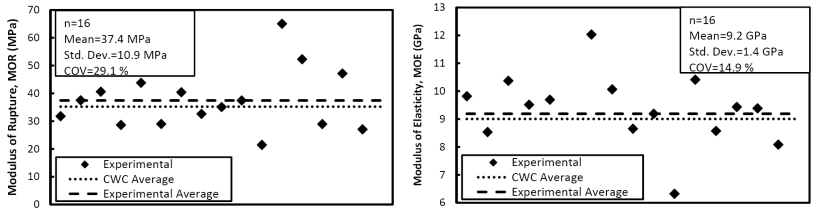

(a) Modulus of Rupture (b) Modulus of Elasticity

Figure 6: Experimental Material Properties from Static Testing.

3.2. Dynamic Results

Figure 7 shows typical failure of four wood specimens after shock tube testing. Figure 7 (a) and (d) show two specimens, 4B and 8A, that have barely reached the point of member failure and returned to a near zero residual displaced shape after testing. Figure 7 (c) and (d) on the other hand show two members, 5A and 6B, which have been severely damaged under shock tube testing. The objective of the dynamic testing was to subject the wood members to a pressure-impulse combination that just achieved incipient failure of the specimens, similar to the response of specimens 4B and 8A and thus enable the accurate calculation of dynamic material properties for wood members. Since shock tube testing method is inherently force controlled, accurately achieving the damaged state shown in Figure 7 (a) and (d) proved to be difficult as the required reflected pressure-impulse combination for failure was unknown. The reflected pressure-impulse generated by the shock tube would normally cause catastrophic failure or leave the specimens relatively undamaged.

(a) Specimen 4B (b) Specimen 5A (c) Specimen 6B (d) Specimen 8A

Figure 7: Four Damaged Wood Specimens after Dynamic Shock Wave Testing.

Figure 8 shows the experimental pressure and displacement-time histories for specimen 4B, 5A, 6B, and 8A recorded during dynamic shock tube testing. The total pressure was applied to the load transfer device over *1.7 m²* tributary area and transferred to the specimen at the loading points. Also shown in the figures are the times to specimen failure or maximum displacement if the specimen did not exhibit distinct signs of failure. These times to failure or maximum displacement were found by analyzing the

displacement and strain-time histories as well as the high speed video. The time to failure or time to maximum displacement was used to determine apparent dynamic member properties.

Figure 8 (a) and (d) show tests that caused very minimal damage to the specimens, 4B and 8A respectively. Specimen 4B was loaded with a maximum reflected pressure of *35.9 kPa* with a positive phase duration of *10.6 ms* resulting in a failure displacement of *39.4 mm* occurring *21.6 ms* after the arrival of the shock front. Specimen 8A was loaded with a maximum reflected pressure of *35.0 kPa* over a *10.6 ms* positive phase duration. The maximum displacement of *36.2 mm* occurred *22.2 ms* after the arrival of the shock wave. In these tests, splitting of the member over the constant moment region was observed. Both specimens returned to a near zero displacement after testing indicating that the elastic limits of the wood was reached but not significantly exceeded.

Specimen 5A and 6B, shown if Figure 8 (c) and (d), respectively, were significantly damaged under the applied shock wave loading. Specimen 5A was loaded with *45.1 kPa* reflected pressure over a *11.6 ms* positive phase resulting in a failure displacement of *37.8 mm* at *14.4 ms* after the arrival of the shock wave. It should be noted that the failure displacement for this specimen was found from the strain-time history as the point of instantaneous change in slope of the curve. Specimen 6B was loaded with a reflected pressure of *36.3 kPa* over a positive phase of *11.5 ms* resulting in failure at *39.5 mm* mid-span displacement *20.5 ms* after the start of the shock wave loading.

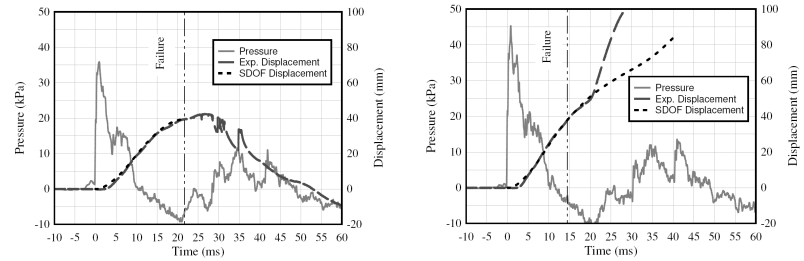

(a) Specimen 4B

(b) Specimen 5A

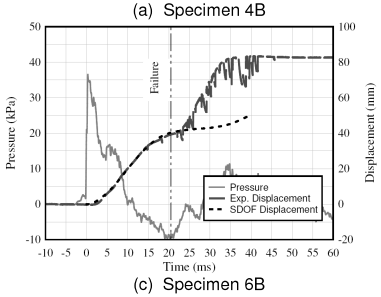

(c) Specimen 6B

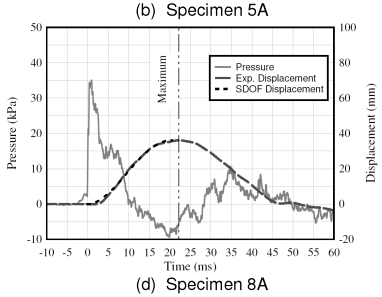

(d) Specimen 8A

Figure 8: Experimental and SDOF Pressure and Displacement-Time Histories.

4. Analysis

An iterative procedure, based on the single-degree-of-freedom (SDOF) method, was used to determine the dynamic resistance curves of the wood specimens tested with the shock tube. These dynamic resistance curves were used to determine the dynamic modulus of rupture and dynamic modulus of

elasticity of the wood beams subjected to high strain-rate loading. Details of the methodology are described below.

4.1. Single Degree of Freedom Method

The wood specimens and load transfer device were modelled as a single–degree-of-freedom oscillator. The equivalent ordinate was taken as the in-plane lateral displacement at the mid-span of the wood beams. The equation of motion used to describe the dynamic response of the simply-supported wood beams subjected to shock wave loading is as follows:

[5] $$k_{LM} m_t \ddot{u}(t) + K_{SDOF} u(t) = A_{LTD} P_r(t)$$

where k_{LM} is the load-mass factor, m_t is the total mass of the system (including wood and load transfer device), K_{SDOF} is the elastic stiffness of the wood beam, A_{LTD} is the loaded area, $P_r(t)$ is the reflected pressure-time history, and $\ddot{u}(t)$ and $u(t)$ are the acceleration and displacement of the mid-span of the system, respectively. It should be noted that any viscous damping is ignored in this calculation since the primary concern of the member response is only up to the first peak in the displacement-time history. This, along with the relatively small damping coefficient associated with structural members, allows for accurate calculations without considering damping (UFC 03-340-02, 2008). The load-mass factor, $k_{LM}=0.87$, for elastic response of a simply supported beam under four point bending with mass lumped at the locations of the point loads. The mass of the load transfer device and wood specimen was calculated as $m_t=101.8\ kg$. The loaded area, A_{LTD}, was $1.7\ m^2$.

In Equation 5, the inertia force of the load transfer device is assumed to be directly proportional to that of the wood specimen itself. In other words, the total mass, m_t, of the system is equal to the mass of the load transfer device plus that of the wood and the displacement and its derivatives are the same for both the load transfer device and the specimen. Since the load transfer device has zero in-plane stiffness, the stiffness term of the equation of motion is only that of the wood specimen itself. The load transfer device has been found to act on the specimen throughout the positive phase duration up to maximum displacement (Lloyd, 2010).

The solution to the SDOF time domain analysis was performed using the average acceleration method (Biggs 1964) with a time step of 10^{-6} seconds. The analysis was run until maximum displacement was calculated.

4.2. Iterative Calculation of Dynamic Wood Properties

The dynamic equation of motion given in Equation 5 was employed in a novel iterative procedure to determine the dynamic MOE and MOR of the wood beams. The total mass and loaded area in Equation 5 were measured prior to testing whereas the applied pressure and displacement (and, indirectly, the acceleration by double differentiation of displacement) were measured experimentally during shock tube testing. Furthermore, time and corresponding displacement at failure or maximum response of the wood beams could be determined from the experimental strain-time and displacement-time histories. The remaining unknown quantity in the equation of motion is the stiffness of the wood beams, K_{SDOF}, which was not recorded during testing. Based on all other known quantities, an iterative SDOF procedure was employed to determine the unknown stiffness of the beams. The dynamic stiffness was computed such that the predicted displacement-time history was in agreement with the experimental displacement-time history up to the time of failure or maximum response.

The dynamic modulus of elasticity for each specimen was also determined by an iterative solution to the single-degree-of-freedom equation of motion given in Equation 5. Based on the linear relationship between applied load and displacement observed during static testing (Figure 5), the wood specimens were modelled with constant stiffness until failure. The apparent dynamic stiffness, K_{SDOF}, was iteratively determined to ensure that the maximum predicted displacement at the time of experimental specimen failure was equal to the corresponding experimental displacement at failure.

The apparent dynamic stiffness was then used to compute the dynamic modulus of elasticity and modulus of rupture by the following formulae:

$$[6] \quad MOE_{dynamic} = \frac{K_{SDOF} a(3L^2 - 4a^2)}{48I}$$

$$[7] \quad MOR_{dynamic} = \frac{24 MOE_{dynamic} \delta_{\max} y}{3L^2 - 4a^2}$$

where $MOE_{dynamic}$ is the dynamic modulus of elasticity based on the iterative SDOF stiffness, δ_{max} is the displacement at the time of failure or maximum response and y is the distance from the neutral axis to the extreme tension fibre (assumed to be $d/2$ as the specimens exhibit essentially elastic behaviour up to failure).

In Figure 8 the solution to the equation of motion of the SDOF system is shown along with the experimental displacement-time histories for specimens 4B, 5A, 6B, and 8A. These plots show that excellent agreement up to the time of maximum response between the experimentally recorded displacement-time histories and those that were generated from the SDOF analysis using the iterative procedure for the apparent dynamic stiffness.

4.3. Apparent Properties

Table 1 presents the dynamic MOE and dynamic MOR calculated for the wood test specimens presented in this paper. Also presented are the ratios of dynamic-to-static properties of wood for the MOR (DIF_{MOR}) and the MOE (DIF_{MOE}).

Table 1: Apparent Dynamic Properties

Specimen	MOR (*MPa*)	MOE (*GPa*)	Failure Strain (*%*)	Strain-rate (s^{-1})	DIF_{MOR}	DIF_{MOE}
4B	51.2	9.9	0.52	0.24	1.37	1.08
5A	55.5	11.2	0.50	0.34	1.48	1.22
6B	50.9	9.8	0.52	0.25	1.36	1.07
8A	59.6	12.6	0.47	0.23	1.59	1.37

The strain in the extreme fibre at failure was found using the dynamic MOR and MOE. The average strain-rate for common building materials, such as concrete and steel is typically taken as the strain at peak load resistance immediately following the initial ascending branch of the force-deformation relationship divided by the time to reach this level of strain (UFC 03-340-02, 2008). Using this definition, the average strain-rates for these specimens are reported in Table 1. Of significance is the DIF_{MOR} for MOR, as this quantity is needed to establish the design strength of material. The limited test data given in Table 1 indicates a minimum value of *1.36* for DIF_{MOR} for a strain rate of *0.24* s^{-1}. The values for the DIF_{MOR} presented in Table 1 are similar in magnitude to those presented in the literature. In 1945 Brokaw and Foster reported an increase in ultimate stress up to *125 %* for Sitka spruce in flexure with times to failure between *50* and *100 ms* (Gerhards, 1977). Considering the lower times to failure reported in this paper, a slightly higher dynamic increase factor is reasonable.

It is important to note that DIF values are from a limited number of tests and are provided as guidance to designers and researchers. Factors such as section size, shear span length, different high strain-rates, and variable moisture content have not yet been explored. The values reported in this paper are similar to those found for the remaining specimens from this test regimen (Jacques et al., 2011). Experimental and analytical research on this topic is ongoing and future publications will present more detailed information on dynamic increase factors for wood.

5. Conclusions

A series of static and high strain-rate bending tests on S-P-F Stud grade wood specimens under four point bending have been performed. These tests were undertaken with the goal of investigating the high strain-rate dependent behaviour of wood. Some of the results of four specimens from the dynamic test program were compared with the static test results. The following conclusions were drawn based on this research:

- A shock tube and load transfer device can be effectively used to generate high strain-rate response in wood beams.
- A high speed data acquisition system with appropriate instrumentation (i.e. strain gauges, LVDTs, pressure sensors, etc) can effectively capture the behaviour of wood beams at high strain-rates.
- SDOF models can be used to accurately predict the behaviour of the wood beams and the load transfer device up to the time of maximum response.
- There was an increase in the modulus of rupture and modulus of elasticity for the specimens tested under dynamic loading.
- A minimum DIF_{MOR} of 1.36 was observed for a strain-rate of 0.24 s^{-1}.

The specimens discussed in this paper exhibited an increase in stiffness and strength over corresponding static values. Although this may be the general behaviour of wood under high strain-rates, the data set provided in this paper is too small to use for design.

6. References

Barrett, J.D. and Lau, W. 1994. *Canadian Lumber Properties*. Canadian Wood Council, Ottawa, Ontario

Biggs, J. M. 1964. *Introduction to Structural Dynamics*. McGraw-Hill, New York, NY.

Bischoff, P. H., and Perry, S. H. 1995. Impact behaviour of plain concrete loaded in uniaxial compression. *Journal of Engineering Mechanics,* 121(6), 685-693.

Gerhards, C. H. 1977. Effect of Duration and Rate of Loading on Strength of Wood and Wood-Based Materials. *USDA Forest Service Research Paper FPL283*, U.S. Department of Agriculture, Forest Service, Forest Products Laboratory, Madison, Wis.

Jacques, E., Lloyd, A., Abdelalim, O., Braimah, A., Doudak, G., and Saatcioglu, M. 2011. Tests of Stud and No. 2 Grade 2x6 Wood Beams under Static and Shock Tube Loading. *Research Report*, Ottawa-Carleton Institute for Civil Engineering, Ottawa, Ontario

Karacabeyli, E. and Barrett, J.D. 1993. Rate of loading effects on strength of lumber. *Forest Products Journal*. 43(5):28-36

Malvar, L. J., and Crawford, J. E. 1998. Dynamic Increase Factors for Steel Reinforcing Bars. *Proceedings of the Twenty-Eighth DDESB Seminar*, DoD Explosives Safety Board, Orlando, FL.

Malvar, L. J., and Ross, C. A. 1998. Review of Static and Dynamic Properties of Concrete in Tension. *ACI Materials Journal*, 95(6), 735-739.

Lloyd, A. 2010. *Performance of reinforced concrete columns under shock tube induced shock wave loading*, Master's thesis, University of Ottawa, Ottawa, Ontario.

Unified Facilities Code (UFC) 03-340-02. 2008. *Structures to Resist the Effects of Accidental Explosions*, United States of America Department of Defense, Washington, D.C.

Congrès annuel 2008 de la SCGC
CSCE 2008 Annual Conference

Québec, QC
10 au 13 juin 2008 / *June 10-13, 2008*

EQUATION FOR THERMAL PROFILE OF NORMAL STRENGTH SILICEOUS AGGREGATE CONCRETE COLUMNS EXPOSED TO FIRE

A. Lloyd[1], R. Wiebe[2] and T. Tikka[3]
[1] Graduate Student, Department of Civil Engineering, University of Ottawa, Ottawa, Ontario Canada
[2] Graduate Student, Department of Civil and Environmental Engineering, University of Waterloo, Waterloo, Ontario Canada.
[3] Department of Civil Engineering, Lakehead University, Thunder Bay, Ontario Canada

ABSTRACT: With the implementation of the 2005 National Building Code, Canada has changed from a prescriptive based code to an objective-based design approach. This change gives designers more freedom to use alternative methods for determining acceptable solutions to meet the minimum specified performance criteria. In the case of fire resistance design, one such alternative to the existing prescriptive solution is to use the temperature, stiffness, and strength relationships of structural materials to compute the fire resistance of a structural member. This study presents a relatively simple method of determining the temperature at any point along the centre line of the cross section for a siliceous-aggregate based, square, tied, steel-reinforced concrete column that is subjected to either the ASTM E119 or the ISO 834 standard fire curve. The temperature profiles from a finite element modeling (FEM) analysis were first developed and compared to physical tests gathered from published literature. A series of temperature profiles for different sized cross sections was then generated using FEM. An equation was developed by using regression analysis techniques to fit the generated temperature profiles. The product of this exercise results in an equation that provides at least the same accuracy as a more robust finite element transient heat transfer model.

1. INTRODUCTION

Exposure to elevated temperatures due to fire causes a reduction in the strength and stiffness of both concrete and steel. In reinforced concrete columns, fire exposure may also lead to spalling of unconfined concrete. Currently the National Building Code of Canada (2005) specifies that a reinforced concrete column be designed according to limit states design and then a specific amount of concrete cover be provided to satisfy the required fire rating. This practice assumes that during a fire, the concrete inside the lateral ties and longitudinal reinforcing steel will retain the design strength and the concrete cover will provide no additional strength or stiffness. The 2005 National Building Code also allows an objective based approach to design, which allows engineers to use alternative solutions so long as they meet the design objective. In the case of fire design the National Building Code states “An objective of this code is to limit the probability that, as a result of the design or construction of the building, a person in or adjacent to the building will be exposed to an unacceptable risk of injury due to a structural failure.” One such alternative solution would be to calculate the temperature profile of the column cross section and determine the corresponding strength and stiffness for a prescribed fire duration. As long as the concrete does not spall and the column has sufficient capacity for the fire duration, the column meets the objective.

The challenge with determining the temperature in a reinforced concrete column is that the transient heat transfer relationship is quite complicated and generally requires the use of numerical method solutions such as finite element or finite difference. This study introduces a relatively simple set of equations for

determining the temperature at any point along the centre line of a square reinforced concrete column exposed to an ASTM E119 (1998) or ISO 834 (1975) fire. These equations that will provide the same accuracy as a robust finite element or finite difference analysis.

2. GOVERNING EQUATIONS OF TRANSIENT HEAT TRANSFER

Heat transfer, in general, is three-dimensional, however, in the case of columns where the length is considerably greater than the cross section dimensions a two-dimensional heat transfer model can be used. A reinforced concrete cross section exposed to fire is subjected to four modes of heat transfer. These modes are surface thermal radiation, conduction, surface convection, and body convection through moisture transport. It is an acceptable practice (Eurocode 2 2006) to ignore the effects of moisture transport as a minor heat transfer contributor and to assume that the conductivity is isotropic (ie. (k_x=k_y=k). These approximations reduce the complexity of the heat transfer model and allows the system to be described by a non linear, non-homogeneous, two dimensional second order partial differential equation (Eq [1], Ahmed and Hurst 1999).

$$[1] \qquad \frac{\partial}{\partial x}\left(k\frac{\partial T}{\partial x}\right)+\frac{\partial}{\partial y}\left(k\frac{\partial T}{\partial y}\right)+q=\rho c\frac{\partial T}{\partial t}$$

Equation [1] describes the heat transfer in two dimensions (x,y) in a medium exposed to a heat source (q) given the temperature (T) dependent material properties of conductivity (k_x=k_y=k) and thermal capacity (ρc).

The heat source term, q, represents the surface flux and is the combination of thermal radiation and convection for the case of reinforced concrete exposed to fire. It is well established that the convection component is an insignificant heat source when compared with the thermal radiation component and may be ignored rendering the source term as exclusively surface radiation as shown in Eq. [2] (Alham 2000).

$$[2] \qquad q=\varepsilon\sigma\left(T_f^4-T_s^4\right)$$

Where ε is the emissivity, σ is the Stefan-Boltzmann constant, T_f is the fire temperature and T_s is the surface temperature of the column.

2.1 Coupled Thermal-Mechanical Analysis

During a fire the thermal and mechanical behaviour of the column are dependent on each other. Thermal behaviour is dependent on mechanical stresses and strains, as these may open or close gaps and slightly change the geometry of a section. So long as the stresses do not cause spalling the mechanical effect on the thermal properties is negligible and may be ignored. However, mechanical stresses and strains are strongly dependant on thermal behaviour, as material strength and stiffness change with temperature. Hence, a thermal analysis may be completed on its own, while a strength analysis must be coupled with the thermal solution.

3. FINITE ELEMENT MODELING

The thermal analysis of a series of reinforced concrete cross sections was completed using a commercially available finite element analysis software (Abaqus 2006) which uses finite element spatial integration for the left hand side of Eq [2], and an implicit backwards difference time step with a lumped capacitance matrix for the right hand side of Eq [2]. This software was chosen because it is capable of running an uncoupled transient heat transfer analysis with non-linear material properties.

All models were created as two dimensional quarter sections using symmetry (Figure 1). A two dimensional model was used because the column is long enough to ensure the thermal gradient along

the length approaches zero. Use of a quarter-section model is possible when both geometric symmetry and symmetric fire exposure are present, as was the case in all of the models studied. Fire loading was applied to the outside edges, while the edges along the lines of symmetry were left unexposed, producing a net heat flow of zero across the lines of symmetry.

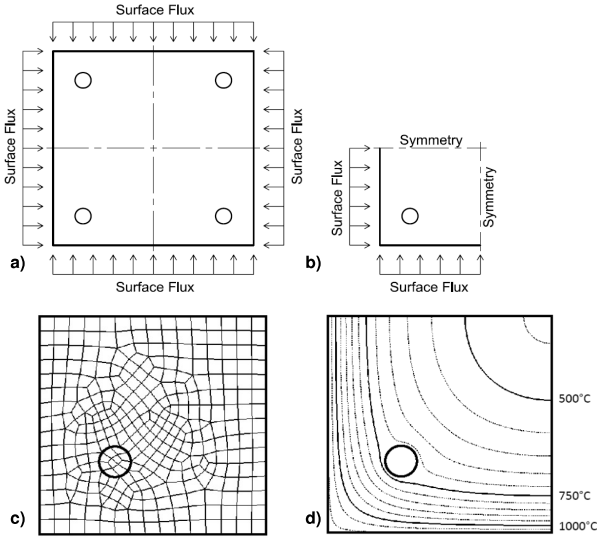

Figure 1 – Cross section of reinforced concrete column studied: (a) cross section of column with surface heat flux; (b) quarter section model of column; (c) typical finite element mesh of quarter section; (d) example thermal profile of quarter section during fire.

The analysis with finite elements is performed over multiple steps. The initial step compiles the physical model geometry and material properties. The geometry is independent of temperature; while the material properties, thermal capacity and conductivity, are defined as tabular temperature dependent values. The other steps in analysis include the application of the boundary conditions and the thermal loading. The boundary conditions are simply the initial internal temperature of the cross section elements. The initial temperature conditions are set by applying a steady state thermal flux to the interior of the cross section components. This flux is removed at the start of the transient analysis to allow the material temperature to vary with the applied fire loading. Thermal radiation equal to the magnitude of the ASTM E119 (1998) fire curve was applied to the surface of the model. There was no applied convection loading. The thermal radiation curve was entered as tabular time dependent values. The software uses a self-adaptive algorithm for the selection of the time step. An initial time step value of 0.1 second and a maximum time step of 300 seconds were specified.

An eight node rectangular bi-quadratic two dimensional solid heat transfer element was used to provide an accurate representation of the temperature dependent material properties across an element. The element size was allowed to vary across the section in order to accurately model the longitudinal steel reinforcing bars and to create a finer mesh in this critical exterior region of the cross section.

3.1. Comparison of Finite Element Analysis with Experimental Results

To test the accuracy of the finite element model, the temperatures computed by the finite element model were compared to temperatures for 20 physical tests, available in the literature (Lie and Woollerton 1988; Wu and Lie 1992; Wu, Lie, and Han 1993). Figure 2 compares the time temperature curves computed from the finite element analysis with the data from four of the physical tests for siliceous aggregate reinforced concrete columns. All of the columns were exposed to a fire with temperatures following ASTM E119 (1998) fire curve. The time-temperature curves shown in these figures are taken at three different thermocouple locations (depths) in each column. Each column has one thermocouple within 38mm of the surface, one thermocouple between 64mm and 101mm from the surface and one thermocouple at the centre. All of the thermocouples were placed along the centre line of the cross section. This thermocouple spacing gives a good sense of the accuracy of the finite element solution throughout the entire column.

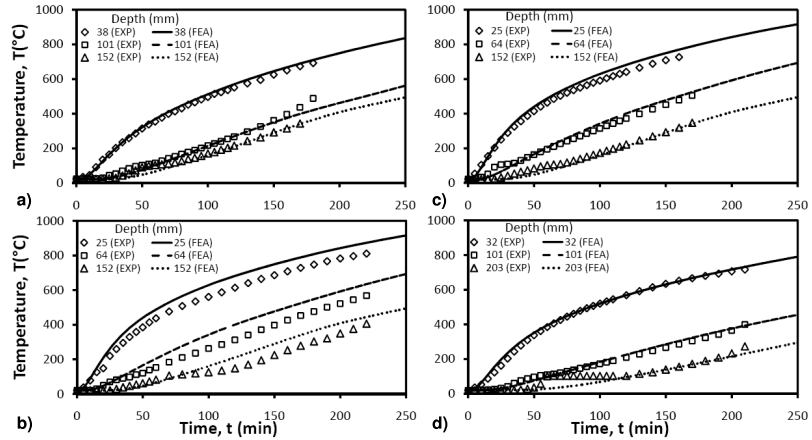

Figure 2. Comparison of experimental and finite element analysis time-temperature curves at varying depths (Lie and Woollerton 1988): (a) 305mm square; (b) 305mm square; (c) 305mm square; (d) 406mm square.

Figure 2 shows a somewhat anomalous behaviour (bump in the data plot) in the experimental test data recorded at the two interior thermocouples occurring at a temperature slightly above 100°C and is due to vapour diffusion and latent heat of vapourization effects. As the water in the concrete is heated a pressure gradient forms which drives the moisture deeper into the section and contributes to the heating of the section. When the temperature-pressure relationship reaches the vapourization point of the water, all heat energy entering the system is devoted to the vapourization process and the surrounding material will not increase in temperature until this process is complete (Ahmed and Hurst 1999). The increased heating rate followed by long periods of vapourization is evident in the time-temperature curves for the experimental data for the thermo couples located at the center of each column in Figure 2. As expected the effects also become more pronounced with depth; the centre thermocouples all have higher initial temperature spikes followed by longer lag times. The temperature readings from the thermocouples near the surface correspond closely with the results from the finite element analysis, because they do not experience the vapourization effects. The interior thermocouple readings also begin to converge with the computed results at temperatures above the vapourization temperature.

The finite element analysis solutions generally follow the shape of the measured time-temperature curves shown in Figure 2. This figure shows that the calculated temperatures are slightly overestimating temperatures, which may be explained by the moisture content effects discussed earlier. Some of the test columns such as the one shown in Figure 2(b) had larger differences in measured vs. computed temperatures. These differences may be caused by a variation in thermocouple placement (ie. actual versus theoretical location), high moisture content, or simply natural variation in concrete properties and performance from one sample to the next.

The temperatures computed from the finite element analysis (T_{FEA}) were compared with 391 experimentally measured temperatures (T_{EXP}) in Figure 3(a). The comparison is for all of the thermocouples reported in the literature, taken at time intervals of 45, 60, 90, 180, and 240 minutes, and at different depths along the centerline of the concrete cross section. An average value of 1.07 and coefficient of variation of 19.4% were computed for ratios of computed to experimental temperatures (T_{FEA}/T_{EXP}). Note, that a temperature ratio (T_{FEA}/T_{EXP}) greater than 1.00 signifies that the temperatures computed from the finite element analysis (T_{FEA}) are conservative when compared to the experimental tests (T_{EXP}). The time-temperature curve comparisons (Figure 2) and statistical evaluations inset in Figure 3(a) indicate that the finite element model computes the temperatures profiles of reinforced concrete columns with reasonable accuracy.

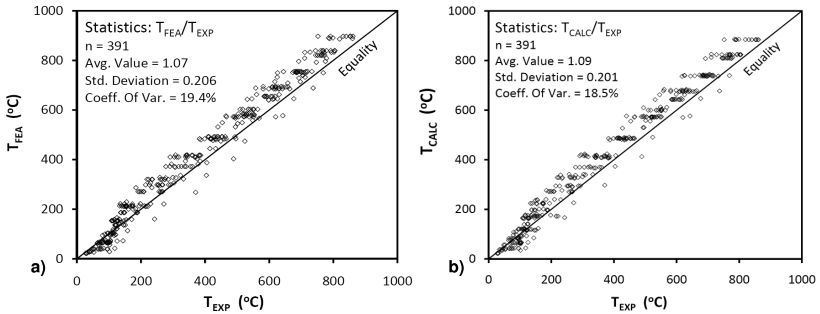

Figure 3. Comparison of experimental temperatures (T_{EXP}) for thermocouples located along the center-line of square reinforced concrete columns with: (a) Temperatures computed with finite element analysis (T_{FEA}); (b) Temperatures computed with Eq. [3] (T_{CALC}).

4. SIMULATION OF THEORETICAL TEMPERATURE PROFILES FOR COLUMNS STUDIED

To evaluate the temperature profiles with respect to time, 28 isolated concrete columns were simulated with each column having a different combination of cross section properties. The columns were subjected to a standard fire as specified by ASTM E119 (1998). The column cross section dimensions and corresponding longitudinal steel ratios ρ_{rs} are listed in Table 1. The seven cross section sizes listed, most representing common sizes used in the construction, were selected in order to determine the effect of cross section size on thermal profiles. Table 1 shows the longitudinal reinforcing steel ratio ranging from zero to eight percent with above four percent representing lap splice regions of heavily reinforced columns. The clear concrete cover to the longitudinal reinforcing steel was held constant at 40 mm. The material thermal properties for the reinforcing steel and siliceous aggregate concrete are given by Zhu and Lie (1993). Siliceous aggregate concrete was used for this study because it has a higher thermal conductivity and a lower specific heat than carbonate aggregate concrete and therefore represents a more conservative temperature model (Zhu and Lie 1993).

Table 1. Sizes and longitudinal reinforcement ratios of columns modeled in study

Column Size (mm)	ρ_{rs} (%)
800	0; 2.2; 3.5; 4.7; 6.6
700	0; 2.1; 3.9; 5.8; 7.9
600	0; 2.0;4.1; 6.0; 7.6
500	0; 2.2; 4.0; 8.0
400	0; 2.1; 5.9
300	0; 1.7; 6.6
250	0; 2.3; 7.5

5. EQUATION FOR THERMAL PROFILES OF SILICEOUS AGGREGATE CONCRETE COLUMNS

For determining the fire resistance of reinforced concrete columns it is desirable to know the temperature at various depths inside the cross section for specific fire durations. The objective of this study is to develop relatively simple equations to determine the temperature with respect to time for any depth along the centre line of a siliceous aggregate based reinforced concrete column that is subjected to the ASTM E119 (1998) fire or the ISO 834 (1975) fire. The equations were developed by using a finite element model to generate temperature profiles across different sized cross sections and applying regression techniques to fit a general equation to the temperature profile curves.

The general shape of a thermal profile of the concrete section shown in Figure 4 is similar to an inverse power function. A modified form of the Richard-Abbot Function (1975) was used to develop the base equation, Eq [3].

$$[3] \qquad T = T_s - T_s\left[1+\left(\frac{\theta_s}{d}\right)^n\right]^{-\frac{1}{n}} \quad , \; T \geq 20^o C$$

In Eq. [3] T is the temperature (°C) at a specific depth and time, d is the depth (mm) from the surface along the centre line to the point of interest, and T_s is the surface temperature (°C) of the column at a specific time. The parameter θ_s is the depth (mm) of the initial tangent of the T *vs.* d curve when projected to the normal ambient temperature (20°C) intercept at a specific time, and n is a parameter describing the magnitude of curvature of the T *vs.* d curve at a specific time. Equation [3] was developed using a base 800mm square column. This equation is only valid for square, siliceous aggregate, reinforced concrete columns between 250mm and 800mm in width.

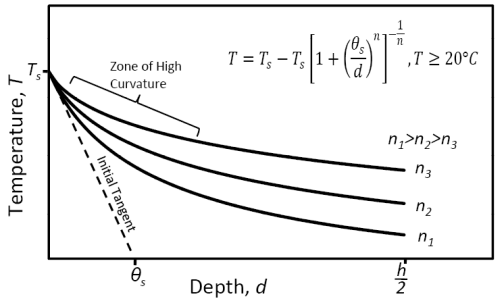

Figure 4. Components of thermal profile curves using Eq. [3].

The surface temperature of a square column is essentially independent of its size when heated on all four sides. Surface temperature is a function of the applied thermal loading and the amount of energy absorbed by the surface. Equation [4] gives the surface temperature of a reinforced concrete column as a function of time, t (minutes), which is always less than the actual fire temperature due to emissivity, the material's conductivity, and the materials specific heat. It was developed by first plotting the surface temperature at the line of symmetry against time for all of the different sized columns, modeled using finite element analysis, for times between 15 and 480 minutes. A logarithmic regression of the simulated values for surface temperature generated from finite element analysis was conducted to obtain the coefficients for Eq. [4].

[4] $$T_s = 180 \times \ln(1.75t)$$

The initial tangent slope of the temperature-depth relationship is largely independent of column size. This relationship is a function of the material properties of the concrete, the applied heat, and the exposure time. To determine the initial projected tangent depth, θ_s, the graph of T *vs.* d was plotted for various times using the base 800mm column. The value of d at the point where the initial tangent intercepts the normal temperature (20°C) is θ_s, as shown in Figure 4. The function $\theta_s(T_s,t)$ was found to be closely related to an inverse power function. Equation [5] is the result of conducting a regression analysis of this function using simulated data from the seven column sizes shown in Table 1.

[5] $$\theta_s = \frac{T_s}{70}\left(t^{\frac{1}{2.8}}\right)$$

The magnitude of the curvature of the temperature vs. depth relationship in Eq. [3] is defined by the dimensionless parameter n. This parameter is also used in conjunction with θ_s and T_s to define the location of the curvature and the magnitude of the core temperature of the concrete. The value of n was found by visually fitting Eq. [3] to the finite element data with the aid of a spreadsheet. The value of n was found to be linearly related to time and a column size factor, K. Equation [6] was developed to modify curvature for any given column size.

[6] $$n = Kt + 2$$

The value of K was determined to be a inverse function (Eq. [7]) related to the cross section size of the column, h (mm).

[7] $$K = 2.7 \times 10^{-3} - \frac{2}{h}$$

5.1 Effect of reinforcing steel ratio

The inclusion of longitudinal reinforcing steel in the columns was modeled using the conservative scenario of a minimal concrete cover of 40mm to the longitudinal bars. The bars were arranged with an equal number of bars on all four faces, using typical bar sizes of between 20M and 30M. It was determined that changing bar size had little effect when the reinforcing steel ratio remained constant. Seven different square column sizes ranging from 250mm to 800mm in width were modeled with reinforcing steel ratios ranging from zero to eight percent of the gross cross section area as shown in Table 1.

The results of the finite element analysis shown in Figure 5 indicate that as the reinforcing steel ratio (ρ_{rs}) increases from zero to eight percent a distinct bend appears in the thermal profile curve. To account for this effect the initial slope of the thermal profile was modified by a reinforcing ratio dependant function. Since the surface temperature of the cross section is not affected by the steel content, the projected

tangent depth, θ_s, was modified. The modification of Eq. [5] to include the effects of steel in siliceous aggregate concrete columns is given in Eq. [8].

[8] $$\theta_s = \frac{T_s}{70}\left(t^{\frac{1}{2.8}}\right)(1+\rho_{rs})$$

This equation will produce conservative temperatures for the concrete located between the surface and the longitudinal steel (Figure 5(b)). These figures show that the equations produce results that are very close to the robust numerical solutions. When using this Eq. [8] the steel reinforcing ratio at the critical design location of the column should be used. For example, multiply ρ_{rs} by two in areas of lap splices.

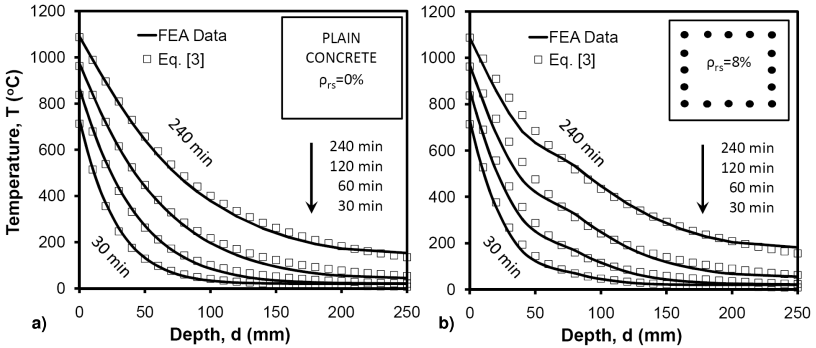

Figure 5. Comparison of thermal profiles from Eq. [3] to finite element analysis results for a 500mm square column using: (a) no reinforcing steel; (b) 8% reinforcing steel

6. COMPARISON OF PROPOSED EQUATIONS WITH PHYSICAL TESTS

Figure 3(b) compares temperatures computed from Eq. [3] (T_{CALC}), using coefficients computed from Eqs. [4], [5], [7] and [8], with the 391 experimentally measured temperatures (T_{EXP}). The comparison is for all of the thermocouples reported in the literature, taken at time intervals of 45, 60, 90, 180, and 240 minutes, and at different depths along the centerline of the concrete cross section. The experimental data is the same set of data that was used earlier in this study for the comparison with the finite element analysis results in Figure 3(a) and the related statistics. Figure 3(b) shows that, overall, Eq. [3] produces slightly conservative temperatures when compared to the experimental data.

The average temperature ratio (T_{CALC}/T_{EXP}), given inset in Figure 3(b), of 1.09 is more conservative than the average of 1.07 obtained form the comparison with the finite element analysis. On the other hand, the coefficient of variation of the temperature ratio from Eq. [3] (18.5%) is lower that the value obtained from the finite element analysis (19.4%).

7. EFFECT OF DEPTH AND TEMPERATURE ON TEMPERATURE RATIOS

The effects of depth and temperature on the average values and the coefficient of variation for temperature ratios (T_{CALC}/T_{EXP}) obtained from Eq. [3], using coefficients computed from Eqs. [4], [5], [7] and [8], are shown in Figure 6. The temperature ratios were examined in groupings of three depth ranges (Figure 6(a)) and three temperature ranges (Figure 6 (b)) with each grouping divided into sets of fire

exposure times. These two ranges are somewhat dependant, as the interior of the column will have mostly cool temperatures while the surface will have mostly high temperatures. The statistics are summarized in Figure 6 and show:

1) The proposed equations have lower variability (coefficient of variation less than 5.5 percent) near the surface and in the high temperature range (>500ºC). This temperature range is important for a designer because it is above 500ºC where the strength and stiffness of concrete and steel begin to decrease at a significant rate (Eurocode 2 2006).

2) The coefficient of variation increases to above 27.7 percent as the depth increases and when the temperature remains below 150ºC. This is likely due to the moisture vapourization and vapour transport effects, which are very difficult to predict. In addition, the sensitivity of the temperature ratio at low temperatures causes a larger variation because a small absolute error will appear large relative to low temperatures.

3) At temperatures between 150ºC and 500ºC the accuracy, as expected, is between that of high and low temperatures.

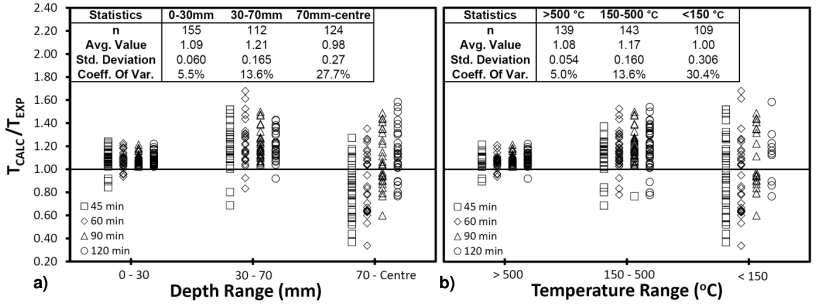

Figure 6. Effects of depth and temperature on temperature ratios computed from Eq. [3] by: (a) depth range; (b) temperature range.

In general, temperatures below 500ºC do not a cause significant strength loss for concrete columns, therefore, any inaccuracy in these equations at lower temperatures is less important (Eurocode 2 2006).

8. SUMMARY AND CONCLUSIONS

This paper presents an evaluation of the major parameters that affect the thermal profiles of square reinforced siliceous aggregate concrete columns that are subjected to a standard ASTM E119 fire curve. The columns were modeled using commercially available finite element software. Simple regression analysis techniques were used to fit an equation to determine the thermal profiles, temperature vs. depth curves at prescribed time intervals, of square normal strength siliceous aggregate reinforced concrete columns exposed to fire. The equation accounts for column size and longitudinal reinforcing steel ratio. The developed equation provides similar results as a finite element analysis and gives the same accuracy as finite element modeling when compared to experimental data.

The equation developed in this study presents the first steps in simplifying heat transfer analysis so that it may be done efficiently by practicing engineers without the need for extensive finite element numerical simulations.

9. ACKNOWLEDEMENTS

The authors would like to thank the Natural Science and Engineering Research Council of Canada (NSERC) for providing financial support for this research.

10. REFERENCES AND STANDARDS

ABAQUS, Inc. 2006, *Abaqus 6.6, Theory Manual.* Providence, RI, USA.

Ahmed, G.N., and Hurst, J.P. 1999. Modeling Pore Pressure, Moisture, and Temperature in High-Strength Concrete Columns Exposed to Fire. *Fire Technology*. Vol. 35, No. 3. 232-262.

Alham, H., 2000. *Development and verification of mathematical models for reinforced concrete encased wide-flanged steel columns exposed to fire.* Ph.D Thesis. Universiti Teknologi Malaysia. Johor Darul Takzim, Malaysia.

ASTM-119-98. 1998. *Standard test methods for fire testing of building construction and materials*. American Society for Testing and Materials. Philadelphia, PA, USA.

Canadian Commission on Building and Fire Codes. 2005. *National Building Code of Canada*. Vol. 1, Twelfth Edition. National Research Council of Canada. Ottawa, ON, Canada.

Eurocode 2: Design of concrete structures. 2006. *Part 1-2: General rules-Structural fire design.* EN 1992-1-2:2006-10. Berlin, Germany.

ISO 834. 1975. *Fire resistance tests-elements of building construction.* International Standard Organization. Geneva, Switzerland.

Lie, T.T., and Woollerton, J.L., 1988. *Fire resistance of reinforced concrete columns: Test results*. National Research Council of Canada, DBR Internal Report No. 569. Ottawa, ON, Canada.

Richard, R.M., and Abbott, B.J. 1975. Versatile elastic-Plastic Stress-Strain Formula. *Journal of the Engineering Mechanics Division*. ASCE. Vol. 101, No. EM4. 511-515

Wu, H.J., and Lie, T.T. 1992. *Fire Resistance of Reinforced Concrete Columns – Experimental Studies*. National Research Council of Canada, IRC Internal Report No. 632. Ottawa, ON, Canada.

Wu, H.J., Lie, T.T., and Han, Q.F. 1993. *Fire Resistance of Reinforced Concrete Columns – Experimental Studies (Conducted at TFRI).* National Research Council of Canada, IRC Internal Report No. 638. Ottawa, ON, Canada.

Zhu, H.L., and Lie, T.T. 1993. *Fire Resistance Evaluation of Reinforced Concrete Columns.* National Research Council of Canada, IRC Internal Report No. 639. Ottawa, ON, Canada.